nature structural & molecular biology

High-resolution structure of TBP with TAF1 reveals anchoring patterns in transcriptional regulation

Madhanagopal Anandapadamanaban[1], Cecilia Andresen[1,6], Sara Helander[1,6], Yoshifumi Ohyama[2], Marina I Siponen[3,5], Patrik Lundström[1], Tetsuro Kokubo[2], Mitsuhiko Ikura[4], Martin Moche[3] & Maria Sunnerhagen[1]

The general transcription factor TFIID provides a regulatory platform for transcription initiation. Here we present the crystal structure (1.97 Å) and NMR analysis of yeast TAF1 N-terminal domains TAND1 and TAND2 bound to yeast TBP, together with mutational data. We find that yeast TAF1-TAND1, which in itself acts as a transcriptional activator, binds TBP's concave DNA-binding surface by presenting similar anchor residues to TBP as does Mot1 but from a distinct structural scaffold. Furthermore, we show how TAF1-TAND2 uses an aromatic and acidic anchoring pattern to bind a conserved TBP surface groove traversing the basic helix region, and we find highly similar TBP-binding motifs also presented by the structurally distinct TFIIA, Mot1 and Brf1 proteins. Our identification of these anchoring patterns, which can be easily disrupted or enhanced, provides insight into the competitive multiprotein TBP interplay critical to transcriptional regulation.

Initiation of eukaryotic gene transcription at a core promoter requires the assembly of a preinitiation complex (PIC). These complexes are biologically dynamic assemblies, and their composition can be altered during development and thereby drive cell-specific programs of transcription[1,2]. All PICs include TATA-binding protein (TBP) and RNA polymerase (Pol I, Pol II or Pol III) as well as polymerase- and promoter-specific coactivators, which include the core factor complex of Pol I, the SAGA or TFIID assemblies of Pol II or the TFIIIB complex of Pol III (refs. 3–6). The megadalton-sized TFIID is a multiprotein assembly and the predominant regulator of protein expression in eukaryotes, comprising TBP and 13 evolutionarily conserved TBP-associated factors (TAFs)[4,5]. TFIID is assembled in a stepwise manner, wherein a symmetric TFIID core complex recruits additional TAFs to form the complete and asymmetric holo-TFIID that nucleates the PIC[7].

TBP is the only protein required for transcription by all polymerases, and mutations in TBP at critical interaction sites suggest that a substantial amount of global gene regulation in yeast and in higher eukaryotes occurs by direct binding to TBP[8,9]. Recent work has structurally described TBP anchoring to the PIC by interactions with general transcription factors Rrn7 (Pol I complex), TFIIB (Pol II complex) or the Brf1 core domain (Pol III complex)[3], enhanced by TFIIA (Pol II complex) or the Brf1 C-terminal extension (Pol III complex)[3] and competitively regulated by NC2 and Mot1 (named BTAF1 in humans)[10]. Direct TBP contacts with a large number of transcriptional activators have long been recognized as a key feature of TBP functionality[5,11,12]. According to the model of 'activation by recruitment', transcriptional activators use separate domains for DNA binding and recruitment of the transcriptional machinery[13]. However, although the DNA anchoring in this model is well established[12], recruiting activation-domain complexes have been characterized only at low resolution[14–17]. Furthermore, although TBP has been shown to be a major target for transcriptional activators[5,8,9,12], no TBP complex with a transcriptional-activating domain has yet been structurally characterized, to our knowledge.

TAF1, with homologs in all eukaryotes, is the largest and functionally most diverse TBP-associated factor and is considered the anchor point for TBP in TFIID[4,5]. Interactions between TAF1 and TBP are required for activated transcription in both yeast and mammalian cells[9]. The so-called 'handoff' hypothesis suggests that TAFs in TFIID help release TBP from autoinhibited or unproductive complexes[8,18,19] and then competitively release TBP to transcriptional activators that take the complex to the promoter[18]. The yeast TAF1 (yTAF1)-TAND1 (residues 10–37) independently acts as a transcriptional-activation domain[18,20], which is functional also when attached to several other TAFs in TFIID[21]. In contrast, the yeast TAND2 region (yTAND2; residues 46–71) independently has an inhibitory effect on transcription[18,20] and competes with TFIIA in binding TBP[22,23]. The *Drosophila* TAF1 (dTAF1)-TAND1 region independently can bind the concave, DNA-binding yeast TBP (yTBP) surface by TATA-box mimicry[24], but it is in itself a very poor transcriptional activator[18]. Although initial NMR data suggest that yTAF1-TAND1 and -TAND2 bind the concave and convex surface of TBP, respectively[20,25], because of the unstable nature of the yTAF1–yTBP complex, its detailed structural features have hitherto not been revealed.

[1]Department of Physics, Chemistry and Biology, Linköping University, Linköping, Sweden. [2]Division of Molecular and Cellular Biology, Graduate School of Nanobioscience, Yokohama City University, Yokohama, Japan. [3]Department of Medical Biochemistry and Biophysics, Protein Science Facility, Karolinska Institutet, Stockholm, Sweden. [4]Ontario Cancer Institute and Department of Medical Biophysics, University of Toronto, Toronto, Ontario, Canada. [5]Present address: Laboratoire de Bioénergétique Cellulaire, CEA Cadarache, Saint Paul lez Durance, France. [6]These authors contributed equally to this work. Correspondence should be addressed to M.S. (maria.sunnerhagen@liu.se).

Received 13 December 2012; accepted 14 May 2013; published online 14 July 2013; doi:10.1038/nsmb.2611

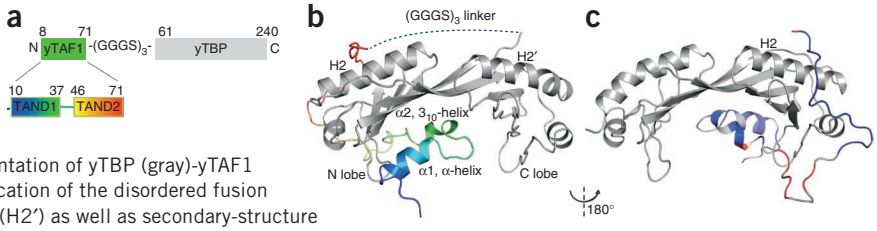

Figure 1 Structure and dynamics of yTBP-yTAF1 binding. (**a**) Schematic representation of yTBP-yTAF1 fusion protein. The yTBP-yTAF1 fusion protein comprises the yTBP core domain and the yTAF1-TAND1 and -TAND2 regions. A $(GGGS)_3$ fusion linker connects the two proteins. (**b**) Cartoon representation of yTBP (gray)-yTAF1 (blue (N) to red (C)), highlighting the approximate location of the disordered fusion linker (dashed line), key yTBP helices 2 (H2) and 2′ (H2′) as well as secondary-structure elements of yTAF1. (**c**) Same as **b**, but rotated 180° in *y* (as indicated) and –55° in *x* and colored by NMR relaxation rates. Residues in yTAF1 with mean R_1 decay rates within ± 2σ of the mean value for yTBP (blue) and >+4σ (red) are shown. ($R_{1\rho}$ and NOE data showing the same pattern are in **Supplementary Fig. 1**.)

To gain specific insight into TBP binding by TAF1, and thereby by transcriptional activators and repressors, we have determined the structure of a biologically active fusion protein comprising the yTBP core domain and residues 8–71 of yTAF1 (ref. 25). By joint use of structural and biological techniques, our work describes the first high-resolution structure, to our knowledge, of a TAF1 protein bound to TBP containing both transcriptionally activating and repressing regions. The current structure and mutational analysis reveals detailed and specific molecular patterns of interactions with TBP, which by their structural diversity and competitive versatility provide an extended basis for the understanding of transcriptional regulation.

RESULTS

Crystal structure of yTBP–yTAF1-TAND1-TAND2

We determined the structure of a biologically fully functional yTBP-yTAF1 fusion protein[25] comprising the yTBP core domain and the yTAF1-TAND1 and -TAND2 regions (**Fig. 1a**) by X-ray crystallography to 1.97-Å resolution (**Fig. 1b** and **Table 1**) and analyzed its dynamics properties by NMR (**Fig. 1c** and **Supplementary Fig. 1**). The fusion $(GGGS)_3$ linker between yTAF1 and yTBP is disordered, as judged by random-coil chemical shifts and complete lack of electron density. While yeast TAND1 (yTAND1) bound yTBP in the DNA-binding groove, yTAND2 bound the convex outer surface of the N-terminal lobe (**Fig. 1b**,**c**). NMR relaxation experiments showed that the yTAND1 and yTAND2 regions are stably anchored toward yTBP while the yTAND1-TAND2 linker region forms a highly dynamic loop-like structure extending from the yTBP core domain (**Fig. 1c**). Although yTAF1 regions that bound yTBP showed similar NMR relaxation decay rates as did yTBP, a result suggesting similar dynamics properties to those of the overall complex, the TAND1-TAND2 linker region showed deviating decay rates suggesting increased flexibility (**Supplementary Fig. 1**). Our NMR relaxation data further supported a stable compact structure of the 1:1 complex in solution with no detectable millisecond exchange (**Supplementary Fig. 1**). Electron density suggested that three tentative Ca^{2+} ions support TBP-TAF1 crystal contacts in this region, but we observed no such bound ions in solution (**Supplementary Fig. 2**). The yTBP structure showed a markedly higher similarity to DNA-bound yTBP (r.m.s. deviation of 0.50) than to dimeric yTBP in the absence of DNA (r.m.s. deviation of 0.93–1.46), whereas each TBP lobe was virtually identical to corresponding lobes in DNA-bound or -free yTBP. Binding of yTAF1 to yTBP thus appeared to stabilize the relative orientations of the N- and C-terminal lobes toward the TATA-bound state (**Supplementary Fig. 3**).

Table 1 Data collection and refinement statistics

	yTBP-yTAF1[a]
Data collection	
Space group	$P2_12_12_1$
Cell dimensions	
a, *b*, *c* (Å)	32.89, 74.25, 99.67
Resolution (Å)	60–1.97 (2.07–1.97)[b]
R_{merge}	0.083 (0.581)
$I / \sigma I$	19.3 (3.2)
Completeness (%)	99.5 (98.3)
Redundancy	7.1 (6.9)
Refinement	
Resolution (Å)	60–1.97
No. reflections	17,873
R_{work} / R_{free}	0.164 / 0.223
No. atoms	
Protein	1,936
Ligand/ion	40
Water	213
B factors	
Protein	26.7
Ligand/ion	49.6
Water	39.5
r.m.s. deviations	
Bond lengths (Å)	0.010
Bond angles (°)	1.020

[a]One crystal was used for data collection and refinement. [b]Values in parentheses are for highest-resolution shell.

TAND1 binds TBP by using buried, TATA box–mimicking residues

The yTAF1-TAND1 region bound the hydrophobic concave surface of yTBP by means of two helices, α1 (residues 16–23) and α2 (residues 30–35; partly a 3_{10} helix), thus occupying the same structural space as the TATA box in the yTBP–DNA structure (**Fig. 2a**). A set of yTAF1-TAND1 residues structurally mimicked DNA bases, riboses and phosphates on both strands of the widened minor groove in yTBP-bound TATA (**Fig. 2b**). Consequently, yTBP contacts to yTAF1-TAND1 also mimicked those to TATA-box DNA[26]. Specifically, residues Phe99, Leu114 and Phe116 of the yTBP N-terminal lobe interacted with Tyr19, Ile22, Ile32, Tyr35 and Ile36 of yTAF1-TAND1, whereas yTBP Val71 and Gln158 from the 'roof' of the TBP concave surface interacted with TAND1 Phe23; all of these yTAF1 residues mimicked base or ribose moieties of TATA-box DNA (**Fig. 2b**). Earlier mutation studies support both TBP residues Val71 and Leu114 as key residues in yTAF1 binding[8,9]. Similarly, interactions mimicking TATA phosphate or base oxygen contacts included yTBP Arg79 and yTAF1 Glu15; yTBP Arg98 and yTAF1 Gly38 (CO); yTBP Asn159 and yTAF1 Ser29 (OH); and finally yTBP Arg196 and yTAF1 Glu26, which together with hydrophobic interactions involving Ile194 and Leu205 of yTBP and Phe27 of yTAF1 connected yTAF1 to the C-terminal yTBP stirrup (**Fig. 2b** and **Supplementary Table 1**). The degree of burial of yTAF1 residues on yTBP binding correlates well with both DNA

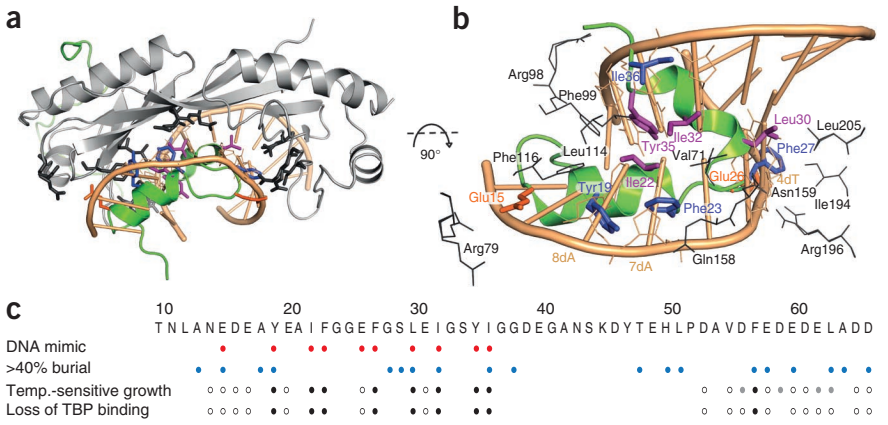

Figure 2 TATA-box mimicry of yTAF1-TAND1. (**a**) Superposition of yTBP (gray)-yTAF1 (green) onto the yTBP–DNA complex (PDB 1YTB; ref. 43; only TATA box is shown). Interacting residues are shown in sticks and colored as below. (**b**) Close-up view of the TAND1 and TBP interaction, with overlaid TATA box as in **a**. Interacting residues in yTBP (gray) and residues in yTAF1-TAND1 mimicking TATA-box riboses (blue), bases (purple) and phosphates (orange) are labeled. The dA and dT of the TATA box are annotated with their position numbers as 8dA and 7dA, and 4dT, respectively. (**c**) DNA-mimicking residues in yTBP–yTAF1-TAND (red) and TAF1 side chains >40% buried in the TBP complex (blue), indicated together with previous results from single-alanine-mutation screening showing temperature (temp.)-sensitive growth and/or lost TBP binding (black dot, severe effects; gray dot, milder effects; empty dot, no effect)[18,29].

mimicking and biological activity, and residues in yTAF1-TAND1 for which alanine mutations impair Gal4-dependent transcription by 70% or more and lead to both temperature-sensitive growth and loss of TBP binding[18] all directly participated in the TBP-binding interface (**Fig. 2c**). The phosphate-mimicking properties of the buried yTAF1 Glu15 may be compensated for in the E15A mutant by neighboring Asp16 and Glu17, thereby reducing the expected negative biological effect of the E15A mutation. Overall, the structure of yTAF1-TAND1 with yTBP was in complete agreement with biological data.

TAND2 binds a TBP surface groove critical for PIC binding

The highly negatively charged yTAF1-TAND2 region (**Fig. 1**), which is required for efficient yTAND1 binding to yTBP[18], bound the yTBP convex surface of the N-terminal lobe, where it meandered through a winding groove traversing helix 2 of yTBP (**Fig. 3a**,**b**). The yTBP groove is lined by positively charged residues including Lys133, Arg137, Lys138, Arg141 and Lys145, which were involved in electrostatic interactions with yTAF1-TAND2 residues Glu60, Glu62, and Asp66 (**Fig. 3b** and **Supplementary Table 1**). Among these, residues Lys133, Lys138 and Lys145 on yTBP helix 2 have been shown to be crucial for interactions within the PICs of Pol I, Pol II and Pol III (refs. 27,28). We observed a network of electrostatic interactions, linking yTBP and yTAF1-TAND2, between the side chains of Glu60, Lys145, Glu62 and Arg141 (**Fig. 3b**). Adjacent to this charge-interaction network, we found a near-complete burial of yTAF1-TAND2 Phe57 in a TBP groove depression, which is lined with aliphatic and aromatic yTBP residues and extended by yTAF1 Val55 (**Fig. 3c**). The backbone of Phe57 was further anchored to TBP by a well-defined hydrogen bond to yTBP Asn91 (**Supplementary Table 1**). Our structural observation of yTAF1 Phe57 as a TBP-anchoring residue is supported by severe growth defects of mutant yTAF1 F57A, comparable in severity to those of a TAND1 deletion[29]. No regular secondary structure formed for yTAF1-TAND2 in its extended interaction with yTBP, but the complex was well formed with low *B* factors.

To investigate the role of the interleaved charge-interaction networks in yTAF1 interactions with the convex yTBP surface, we designed a set of TAND2 mutations. Whereas previous experiments have shown that E60A or E62A alone have little effect on TBP binding[29],

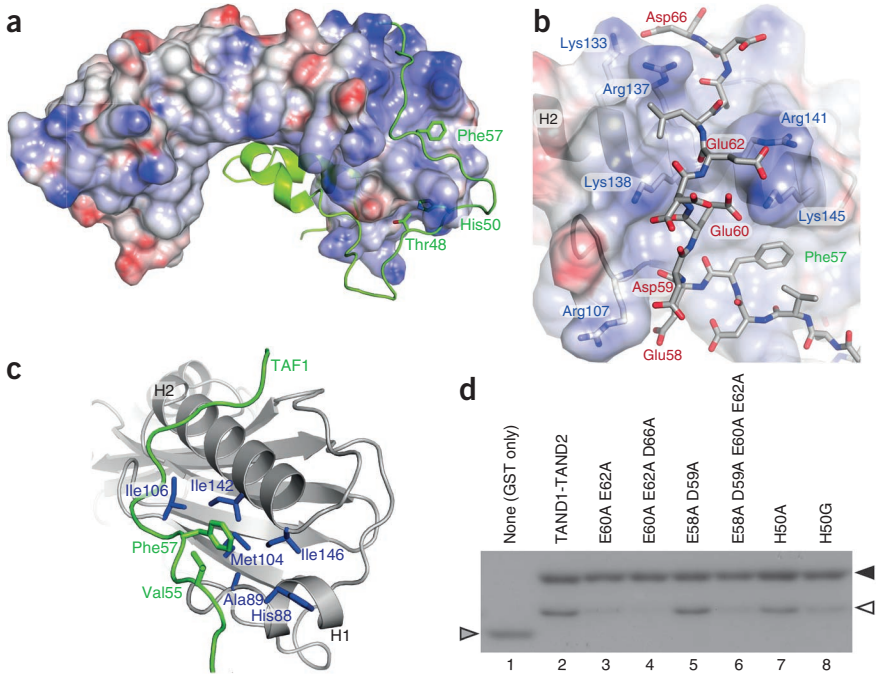

Figure 3 Electrostatic and hydrophobic anchoring of yTAF1-TAND2 to yTBP. (**a**) Electrostatic surface representation of yTBP, with the bound yTAF1-TAND2 in green and with anchoring TAND2 residues annotated. (**b**) Detailed view of the surface-groove interaction connecting yTAF1-TAND2 (sticks) and yTBP (cartoon). Participating side chains in the charge-charge interaction network are shown in sticks and labeled, as is the Phe57 anchor residue. Hydrogen bonds are listed in **Supplementary Table 1**. (**c**) The yTBP hydrophobic surface pocket, lined by residues (blue) in helix 1 (His88 and Ala89), strand 2 (Met104 and Ile106) and helix 2 (Ile142 and Ile146), binding to the anchoring Phe57 residue supported by Val55 in yTAF1-TAND2 (green). (**d**) Glutathione S-transferase (GST) pulldown assays. GST-TAND1-TAND2 fusion proteins carrying TAND2 mutations as indicated (lanes 3–8), wild-type TAND1-TAND2 (lane 2) or GST alone (lane 1) were incubated with equimolar TBP. Arrowheads indicate GST-TAND1-TAND2 (black), TBP (white) and GST (gray) positions.

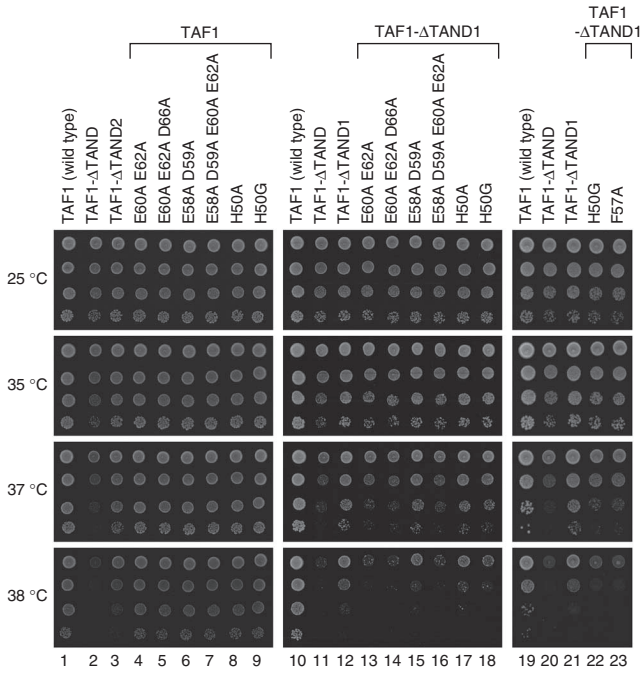

Figure 4 Multiple acidic residues in TAND2 affect yeast growth. Growth phenotype of yeast strains carrying TAND mutations as indicated. Effects of site-specific TAND2 mutations on growth assayed both in the presence (lanes 4–9) and absence (lanes 13–18, 22–23) of TAND1 are shown in strains serially diluted (tenfold), spotted onto YPD medium and grown at the indicated temperatures for 3 d. For direct comparison, a joint experiment with the previously studied F57A mutant[29] is shown.

we found that the double mutation E60A E62A, which would efficiently disrupt the Glu60-Lys145-Glu62-Arg141 network (**Fig. 3b**), indeed drastically reduced both yTBP binding (**Fig. 3d**) and yeast growth rates in yTAF1-ΔTAND1 (**Fig. 4**). Our results suggest a principal role for this charge-interaction network in TAND2-TBP anchoring. In contrast, the double mutant E58A D59A, designed on the basis of its structural interaction with yTBP Arg107 (**Fig. 3b**), did not release yTBP binding (**Fig. 3d**) and had little effect on yeast growth (**Fig. 4**). None of the multiple charge mutants significantly affected yeast growth in intact yTAF1, even when combined, thus suggesting that the charge-interaction networks mainly consolidate yTAF1-TAND2 anchoring (**Fig. 4**). Furthermore, His50 was nearly completely buried in the complex (**Fig. 2c**) and structurally anchored the TAND1-TAND2 linker to yTBP (**Fig. 3a**). H50A did not significantly affect growth, but a mutation (H50G) removing all hydrophobicity released yTBP binding (**Fig. 3d**) and affected yeast growth in a yTAF1-ΔTAND1 strain to a similar extent as did a F57A mutation (**Fig. 4**). Taken together, our experiments suggest three major TAND2 binding determinants: (i) hydrophobic anchoring of Phe57 into the groove on the yTBP convex surface, (ii) a charge-interaction network linking negative charges Glu60 and Glu62 in yTAND2 with positive surface charges Lys145 and Arg141 on yTBP and (iii) burial of His50 in the yTAND1-TAND2 linker region. The yTAF1-TAND2 motif is highly conserved in human TAF1 (hTAF1) and dTAF1 (ref. 29), and we thus expect the TAND2 motifs of hTAF1 and dTAF1 to anchor into the TBP convex surface groove similarly to yTAF1-TAND2.

TAND1 uses the same anchor points as does Mot1, but in reverse

As described above, the yTAND1 region of yTAF1 appeared to disrupt TBP interactions when replaced with DNA-mimicking residues—a strategy that has previously been suggested for both dTAF1 and *Encephalitozoon cuniculi* Mot1 (EcMot1)[10,24]. The interactions of EcMot1 and yTAF1-TAND1 with TBP were particularly similar: EcMot1 Phe123 interacts with *E. cuniculi* TBP (EcTBP) Gln116 similarly to yTAND1 Phe23 with yTBP Gln158, and EcMot1 Phe129 forms an aromatic stack with EcTBP Phe57 and Phe74 in the same way as yTAND1 Tyr19 with yTBP Phe99 and yTBP Phe116 (**Fig. 5a**). Furthermore, a corresponding EcMot1 electrostatic interaction equivalent to that between yTAND1 Glu26 and yTBP Arg196, connecting yTAND1 to the C-terminal yTBP stirrup, is found between EcMot1 Glu120 and EcTBP Lys159 and is further stabilized by the hydrogen bond between EcMot1 His118 and EcTBP Arg154 (**Fig. 5a**).

Notably, a closer look revealed that the peptide-chain orientation of yTAF1 is reversed compared to that of EcMot1 and dTAF1, although both the relative orientation of their helices and the mode of TBP interactions on an individual-residue level are highly similar between the two proteins. Notably, the yTAF1-TAND region could be aligned to the reverse sequence of EcMot1 with TBP-contacting residues in conserved positions (**Fig. 5b**). We also found that transcriptional-activation domains in EBNA2, VP16 and Gal4, which

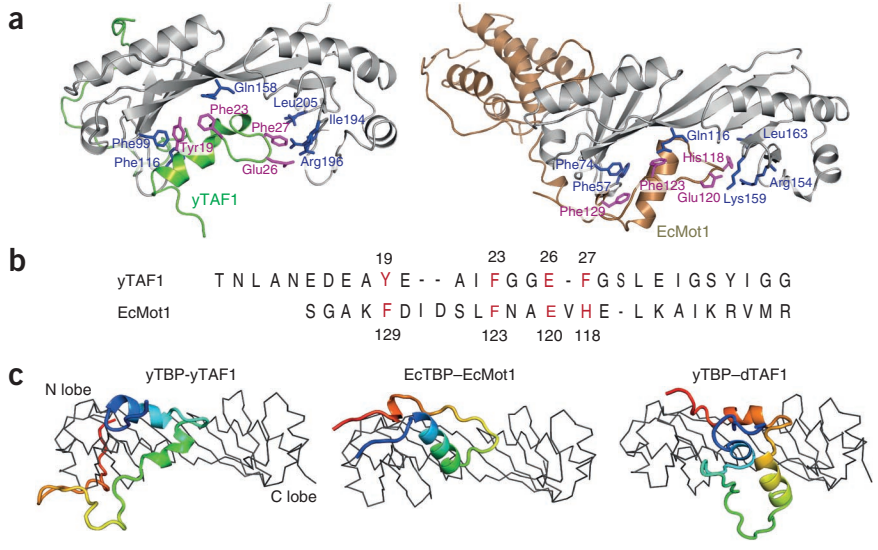

Figure 5 Similar TBP-anchoring residues in yTAF1-TAND1 and Mot1 despite reverse sequence tracing. (**a**) Cartoon representation of TBP complexes with yTAF1 (green, current structure) and EcMot1 (sand, PDB 3OC3; ref. 10), highlighting interacting residues of TBP (blue) and yTAF1 or EcMot1 (magenta). Only part of the EcMot1 structure is shown for clarity. (**b**) Structure-based sequence alignment between the TBP-interacting residues of yTAF1 and EcMot1. TBP-anchoring residues are annotated, and the EcMot1 sequence is reversed as prompted by the reversed structural sequence tracing shown in **a**. (**c**) Ribbon-style representation of TBP and cartoon yTAF1, EcMot1 and dTAF1 (PDB 1TBA; ref. 24) with rainbow coloring (blue, N terminus; red, C terminus). The TBP lobes are labeled, and the orientation is 90° rotated compared to **a**.

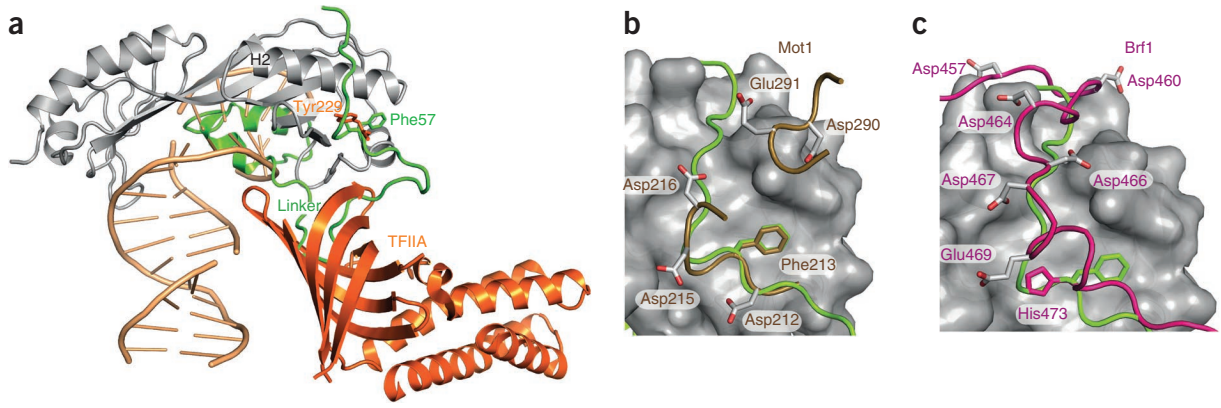

Figure 6 Conserved surface-groove and anchoring residues in competitive TBP binding. (**a**) Superposition of TBP-TAF1 onto the TBP–TFIIA (orange)–DNA (wheat) ternary complex (from PDB 1NH2; ref. 35). Aromatic TBP-anchoring residues of TAF1 and TFIIA on the convex TBP surface are shown as sticks and labeled. The linker region between TAND1 and TAND2 of TAF1 protruding into the space occupied by the β-barrel TFIIA structure is highlighted. (**b**,**c**) TBP complexes with Mot1 (sand, PDB 3OC3; ref. 10) (**b**) and Brf1 (magenta, PDB 1NGM; ref. 31) (**c**) superimposed onto yTAF1 (green)-yTBP (surface), highlighting in stick representation the common anchoring aromatic residue in these transcription activators and repressors as well as hydrogen-binding side chains connecting to the basic region of TBP. All superpositions were made by structural alignment of the TBP backbone in the respective complexes onto yTBP in the current structure, shown in **a**–**c**.

are functionally similar to yTAF1-TAND1 in transcriptional activation and also bind the TBP concave surface[18], could be aligned to yTAF1-TAND1-TAND2 with conserved contact residues to TBP (**Supplementary Fig. 4**). In the dTAF1-yTBP structure, dTAF1-TAND1, compared to yTAF1 and Mot1, covers an extended surface (**Fig. 5c**), consistent with its higher affinity to TBP[29]. However, although several of the yTAF1 and Mot1 contacts to TBP are also found in dTAF1 (ref. 24), the different threading of dTAF1-TAND1 into the TBP DNA-binding groove (**Fig. 5c**) precludes dTAF sequence alignment to yTAF1-TAND1 or Mot1, because, as compared to yTAF1 and Mot1, its DNA-mimicking patches are nonlinearly permutated in sequence. The longer hTAF1 TAND1 motif (residues 1–100) showed sequence similarities to both yTAF1-TAND1 and dTAF1, thus suggesting the presence of two TBP-binding motifs N-terminal to hTAF1-TAND2: one N-terminal motif similar to dTAF1-TAND1 and a second motif resembling yTAF1-TAND1, which is directly connected to hTAF1-TAND2 (**Supplementary Fig. 4**).

TAND2 presents a conserved regulatory TBP-binding motif

The structure of yTBP-yTAF1, together with previous TBP–TFIIA, TBP–Brf1 and TBP–Mot1 structures, gives new insight into the specificity of convex-surface interactions by TBP-binding proteins. TFIIA binding to TBP competes with yTAF1 TBP binding in yeast transcriptional initiation[23,30], but the specific molecular determinants for this have hitherto been unknown. In our structure, we found that yTAF1 anchors into the same TBP convex surface groove as does the acidic loop (228-D**Y**LI-231, with aromatic anchoring site in bold) of TFIIA and, furthermore, wraps around the TBP N-terminal stirrup region in a way that renders simultaneous binding of TFIIA impossible (**Fig. 6a**). A closer analysis suggested direct molecular competition for the aromatic binding pocket between Phe57 of yTAF1 and Tyr229 of TFIIA (**Fig. 6a**). Superimposition of the backbone of the TBP entities in TBP–EcMot1 and yTBP-yTAF1 resulted in structural overlap of Phe213 and Phe57 of EcMot1 and yTAF1-TAND2, respectively, which both inserted into the same hydrophobic cleft in TBP (**Fig. 6b**). The crystal structure of a ternary Brf1–TBP–DNA complex (PDB 1NGM)[31] reveals a similar association of Brf1 in the same surface groove. Brf1 His473 replaces the Phe57 (yTAF1-TAND2) key residue in the corresponding TBP hydrophobic cleft but with a 180° reversal of the side chain orientation in the hydrophobic cleft, possibly due to the main chain running in reverse through the groove (**Fig. 6c**).

Our structure and mutational analysis showed that efficient binding of yTAND2 (55-VD**F**EDEDEDELADD-66) to the yTBP convex surface groove in addition to aromatic anchoring of Phe 57 (in bold) also requires charge-charge interactions between yTAND2 acidic residues (underlined) and conserved lysines and arginines on TBP (**Figs. 3** and **4** and **Supplementary Table 1**). The TAND2 core region is well conserved in yTAF1, dTAF1 and hTAF1, thus suggesting similar TBP binding[29]. Notably, we found that both EcMot1 and Brf1 show similar stretches of acidic residues that interact with the same basic TBP surface as does yTAF1-TAND2. Tracing the same groove but in reverse as compared to TAND2, Brf1 (ref. 31) (457-DDPDNLEDVDDEELNA**H**LLNEE-478) displays acidic residues (underlined) N-terminal to its aromatic histidine anchor residue (bold), interacting similarly as TAND2 with the TBP basic patch (**Fig. 6c**). In EcMot1, acidic residues (underlined) C-terminal to the buried phenylalanine (211-N**D**F**V**DD-216) together with acidic residues from the EcMot1 heat-repeat region (288-SPDEDI-293) jointly match the TBP basic patch (**Fig. 6b**). Finally, although the TFIIA structure does not show electron density beyond the aromatic anchor provided by 228-D**Y**LI-231, mutations of TBP lysines on helix 2 were previously shown to disrupt TBP-TFIIA interactions[27,32], thus suggesting electrostatic contributions to binding. Notably, a 30-fold increase of TFIIA-TBP binding has been observed upon phosphorylation of TFIIA at Ser220, Ser225 and Ser232 (ref. 33) surrounding the aromatic anchor residue, and a S220A S225A S232A multiple mutant protein has shown greatly reduced transcriptional activity[34]. We noted that although structurally disordered in the crystal[35], these residues envelop the 228-D**Y**LI-231 motif that competes with TAF1 binding to the TBP convex surface groove (**Fig. 6**). Extrapolating from our yTAF1-yTBP structure, we propose that phosphorylation of these TFIIA serines could provide the vital negative charge required for interaction with the conserved lysines on TBP (**Figs. 3** and **4**), thus leading to enhanced TBP binding and transcription. Similar structural mechanisms may well govern PTEN-mediated regulation of Brf1, in which phosphorylation controls the association between TBP and Brf1 (ref. 36), and phosphorylation adjacent to a critical tryptophan

residue in the glucocorticoid-receptor transactivation domain AF1 dramatically increases TBP binding[37].

DISCUSSION

The current high-resolution structure of yTBP–yTAF1-TAND1-TAND2 shows how TBP is anchored to the TFIID complex and provides structural details on how an intrinsically disordered transcriptional regulatory yTAF1 domain[20] interacts with TBP. By favoring the presence of the bound state in a fusion protein, in which increased association rates have shifted the equilibrium toward the complex state[25], we could identify and characterize critical anchor points in the TBP-TAF1 interaction by structural and mutational analysis. Induced folding is considered to be a major driving force for interaction between a disordered and a folded protein[38]. For yTAF1 binding to TBP, strong coupling of folding and binding is demonstrated by the near-complete disruption of both binding and biological function upon removal of any single hydrophobic anchoring side chain in yTAF1-TAND1-TAND2 (**Figs. 2**–**4**). The charge-charge anchoring interactions identified on the convex TBP surface are less sensitive to single mutations and seem to contribute to binding in a more additive way with lower levels of structural rigidity (**Figs. 3** and **4**). We find that the anchoring interactions identified in yTAF1 are present also in other structurally diverse TBP-binding general transcription factors (**Figs. 5** and **6**) and may well be widely present in TBP-binding transcriptional-activation domains. In particular, the detailed structural and mutational characterization of the binding of the TAND2 acidic and aromatic peptide regions to the TBP convex surface (**Figs. 3**, **4** and **6**) provides a new molecular framework for addressing the as-yet-unresolved question of how apparently casually assembled charged peptides with key aromatic residues can recruit TBP and thereby activate transcription[11,12].

At first glance, some features of the current structure might seem to reflect suboptimal yTAF1-yTBP interactions, as shown by the structural and sequence diversity of TBP interactors using similar anchor points and the sensitivity of complex formation and biological activity to mutations at these sites. However, we suggest instead that these properties may all be required for biological function because they enable rapid dynamic competition between positively and negatively acting factors binding common TBP-interaction sites. Such competition has been suggested to be a cornerstone for biologically adequate responsiveness in the regulation of transcriptional output[8]. Because TBP is jointly required by Pol I, Pol II and Pol III complexes, a simultaneously selective and dynamic TBP recruitment mechanism is essential to direct alternate usage of Pol I, Pol II and Pol III as biologically required. The structural and sequence divergence in proteins competitively binding identical TBP-interaction surfaces as shown here (**Figs. 2**, **5** and **6**) provides differential handles and thereby a biologically versatile means of differentially directing recruitment of the jointly used TBP into various multiprotein complexes targeting transcription. Targeting of anchoring positions by proteins competing for the same binding site can readily be exploited *in vivo* to direct the timing of biologically appropriate interactions. Such anchoring possesses a biological advantage because multiple TBP binding equilibria can then easily be shifted simply by competition at single sites in the interaction surface, by altered expression levels of competing proteins or by post-translational modifications affecting the affinity of one of the competitors. Efficient and regulated competition at anchoring positions on TBP provides for rapid alteration of cell fate in response to biological needs by directing TBP recruitment to various transcription complexes and promoter sites.

Although the current structure of the stabilized yTAF1-yTBP fusion protein presents a snapshot of the bound state, we know that dynamics in regulatory TBP binding is biologically crucial[8]. In fact, transcriptional activity appears to be inversely correlated with the formation of stable TBP complexes[18]. The yTAF1-TAND1 and the transcriptional-activation domains from EBNA2, VP16 and Gal4, which all form less stable complexes with TBP, are all still able to efficiently activate transcription in a Gal4 assay[18]. In contrast, dTAF1-TAND1, which binds the same TBP surface as does yTAF1-TAND1 but with nanomolar affinity, is unable to activate transcription[29]. Thus, the formation of a stable TBP complex is not consistent with high transcriptional activity; indeed, a complete structural description of an efficient TBP–transcriptional-activator complex may require an ensemble of states[8,14]. In fact, the frequent presence of multiple transcriptionally activating regions with a low degree of sequence homology in the same transcriptional regulator[12] may promote intrinsic multivalent competition. In agreement with the handoff model[13,17,23], such rapid dynamic shielding of critical TBP-binding surfaces might be required to avoid the formation of autoinhibited or unproductive TBP complexes while retaining access for downstream general transcription factors. We hypothesize that competitive conformational exchange at anchoring positions may provide the clue for how TBP, despite its relatively rigid fold as compared to those of other multirecognition proteins[39,40], is able to bind such a wide variety of dynamic interactors in a timely and productive manner.

Taken together, our data on TBP binding extend the view of transcriptional competition of TBP interactors to a common target. In particular, our structure identifies and highlights how TBP-anchoring residues are similarly presented to TBP by varied TBP-interacting folds, in a way that allows for TBP interactions to be easily disrupted or enhanced by competition or by post-transcriptional modification. In biophysical terms, our data agree with transcriptional activation as a highly dynamic process in which ensembles of multiprotein equilibria are shifted as a response to biological signals rather than to a hierarchic initiation of a single-way, sequential cascade of events. Increased or decreased binding of transcriptional regulators may shift the TBP multiprotein equilibria and thereby promote TBP relocation, in agreement with transcription sites being rapidly assembling and disassembling entities. For transactivating domains to interfere in the regulation of such a dynamic entity as the PIC[41], flexibility may be a prerequisite[42]. Increased structural and biophysical knowledge in this area is critical to understanding how transcription factors and transcriptional activators collaborate in regulating the transcription of individual genes as well as entire gene programs.

METHODS

Methods and any associated references are available in the online version of the paper.

Accession code. Atomic coordinates have been deposited in the Protein Data Bank under accession code 4B0A.

Note: Supplementary information is available in the online version of the paper.

ACKNOWLEDGMENTS

This work was supported by the Swedish Research Council (621-2011-6028 and 621-2012-5250 to M.S.; 621-2012-5136 to P.L.), VINNOVA (P32045-1 to M.S.), the Swedish Cancer Foundation (11 0681 to M.S.), the Swedish Child Cancer Foundation (PROJ09/092 to M.S.), the Forum Scientium Award (C.A.), the Canadian Institutes for Health Research (MT-13611 to M.I.), the grant-in-Aid for Scientific Research from Japan Society for the Promotion of Science (23370077 to T.K.) and equipment grants to Linköping University from the Knut and Alice Wallenberg foundation. M.I. is supported as a Canada Research Chair. We thank H.Th.M. Timmers, L. Penn, C.H. Arrowsmith and P. de Graaf for critical discussion and acknowledge the Swedish NMR Centre, the Protein Science Facility and beamline ID14-1 at the European Synchrotron Radiation Facility.

AUTHOR CONTRIBUTIONS
M.I. and M.S. conceived of and designed the study. Experiments and data evaluation were designed and performed by M.A., M.I.S. and M.M. (crystallography), Y.O. and T.K. (yeast mutations) and M.A., C.A., S.H., P.L. and M.S. (NMR). M.A., C.A., S.H., M.M. and M.S. wrote the paper. All authors discussed the interpretation and implications of the results and edited the manuscript at all stages.

COMPETING FINANCIAL INTERESTS
The authors declare no competing financial interests.

1. Goodrich, J.A. & Tjian, R. Unexpected roles for core promoter recognition factors in cell-type-specific transcription and gene regulation. *Nat. Rev. Genet.* **11**, 549–558 (2010).
2. D'Alessio, J.A., Ng, R., Willenbring, H. & Tjian, R. Core promoter recognition complex changes accompany liver development. *Proc. Natl. Acad. Sci. USA* **108**, 3906–3911 (2011).
3. Vannini, A. & Cramer, P. Conservation between the RNA polymerase I, II, and III transcription initiation machineries. *Mol. Cell* **45**, 439–446 (2012).
4. Papai, G., Weil, P.A. & Schultz, P. New insights into the function of transcription factor TFIID from recent structural studies. *Curr. Opin. Genet. Dev.* **21**, 219–224 (2011).
5. Thomas, M.C. & Chiang, C.M. The general transcription machinery and general cofactors. *Crit. Rev. Biochem. Mol. Biol.* **41**, 105–178 (2006).
6. Hahn, S. Structure and mechanism of the RNA polymerase II transcription machinery. *Nat. Struct. Mol. Biol.* **11**, 394–403 (2004).
7. Bieniossek, C. *et al.* The architecture of human general transcription factor TFIID core complex. *Nature* **493**, 699–702 (2013).
8. Chitikila, C., Huisinga, K.L., Irvin, J.D., Basehoar, A.D. & Pugh, B.F. Interplay of TBP inhibitors in global transcriptional control. *Mol. Cell* **10**, 871–882 (2002).
9. Martel, L.S., Brown, H.J. & Berk, A.J. Evidence that TAF-TATA box-binding protein interactions are required for activated transcription in mammalian cells. *Mol. Cell Biol.* **22**, 2788–2798 (2002).
10. Wollmann, P. *et al.* Structure and mechanism of the Swi2/Snf2 remodeller Mot1 in complex with its substrate TBP. *Nature* **475**, 403–407 (2011).
11. Sigler, P.B. Transcriptional activation: acid blobs and negative noodles. *Nature* **333**, 210–212 (1988).
12. Hahn, S. & Young, E.T. Transcriptional regulation in *Saccharomyces cerevisiae*: transcription factor regulation and function, mechanisms of initiation, and roles of activators and coactivators. *Genetics* **189**, 705–736 (2011).
13. Ptashne, M. & Gann, A.A. Activators and targets. *Nature* **346**, 329–331 (1990).
14. Brzovic, P.S. *et al.* The acidic transcription activator gcn4 binds the mediator subunit gal11/med15 using a simple protein interface forming a fuzzy complex. *Mol. Cell* **44**, 942–953 (2011).
15. Liu, W.L. *et al.* Structures of three distinct activator-TFIID complexes. *Genes Dev.* **23**, 1510–1521 (2009).
16. Baek, H.J., Kang, Y.K. & Roeder, R.G. Human Mediator enhances basal transcription by facilitating recruitment of transcription factor IIB during preinitiation complex assembly. *J. Biol. Chem.* **281**, 15172–15181 (2006).
17. Elmlund, H. *et al.* Cryo-EM reveals promoter DNA binding and conformational flexibility of the general transcription factor TFIID. *Structure* **17**, 1442–1452 (2009).
18. Kotani, T. *et al.* A role of transcriptional activators as antirepressors for the autoinhibitory activity of TATA box binding of transcription factor IID. *Proc. Natl. Acad. Sci. USA* **97**, 7178–7183 (2000).
19. Muldrow, T.A., Campbell, A.M., Weil, P.A. & Auble, D.T. MOT1 can activate basal transcription *in vitro* by regulating the distribution of TATA binding protein between promoter and nonpromoter sites. *Mol. Cell Biol.* **19**, 2835–2845 (1999).
20. Mal, T.K. *et al.* Structural and functional characterization on the interaction of yeast TFIID subunit TAF1 with TATA-binding protein. *J. Mol. Biol.* **339**, 681–693 (2004).
21. Takahata, S., Kasahara, K., Kawaichi, M. & Kokubo, T. Autonomous function of the amino-terminal inhibitory domain of TAF1 in transcriptional regulation. *Mol. Cell Biol.* **24**, 3089–3099 (2004).
22. Bagby, S. *et al.* TFIIA-TAF regulatory interplay: NMR evidence for overlapping binding sites on TBP. *FEBS Lett.* **468**, 149–154 (2000).
23. Kokubo, T., Swanson, M.J., Nishikawa, J.I., Hinnebusch, A.G. & Nakatani, Y. The yeast TAF145 inhibitory domain and TFIIA competitively bind to TATA-binding protein. *Mol. Cell Biol.* **18**, 1003–1012 (1998).
24. Liu, D. *et al.* Solution structure of a TBP-TAF(II)230 complex: protein mimicry of the minor groove surface of the TATA box unwound by TBP. *Cell* **94**, 573–583 (1998).
25. Mal, T.K. *et al.* Functional silencing of TATA-binding protein (TBP) by a covalent linkage of the N-terminal domain of TBP-associated factor 1. *J. Biol. Chem.* **282**, 22228–22238 (2007).
26. Kim, J.L., Nikolov, D.B. & Burley, S.K. Co-crystal structure of TBP recognizing the minor groove of a TATA element. *Nature* **365**, 520–527 (1993).
27. Buratowski, S. & Zhou, H. Transcription factor IID mutants defective for interaction with transcription factor IIA. *Science* **255**, 1130–1132 (1992).
28. Kim, T.K. & Roeder, R.G. Involvement of the basic repeat domain of TATA-binding protein (TBP) in transcription by RNA polymerases I, II, and III. *J. Biol. Chem.* **269**, 4891–4894 (1994).
29. Kotani, T. *et al.* Identification of highly conserved amino-terminal segments of dTAFII230 and yTAFII145 that are functionally interchangeable for inhibiting TBP-DNA interactions *in vitro* and in promoting yeast cell growth *in vivo*. *J. Biol. Chem.* **273**, 32254–32264 (1998).
30. Ozer, J., Mitsouras, K., Zerby, D., Carey, M. & Lieberman, P.M. Transcription factor IIA derepresses TATA-binding protein (TBP)-associated factor inhibition of TBP-DNA binding. *J. Biol. Chem.* **273**, 14293–14300 (1998).
31. Juo, Z.S., Kassavetis, G.A., Wang, J., Geiduschek, E.P. & Sigler, P.B. Crystal structure of a transcription factor IIIB core interface ternary complex. *Nature* **422**, 534–539 (2003).
32. Lee, D.K., DeJong, J., Hashimoto, S., Horikoshi, M. & Roeder, R.G. TFIIA induces conformational changes in TFIID via interactions with the basic repeat. *Mol. Cell Biol.* **12**, 5189–5196 (1992).
33. Solow, S.P., Lezina, L. & Lieberman, P.M. Phosphorylation of TFIIA stimulates TATA binding protein-TATA interaction and contributes to maximal transcription and viability in yeast. *Mol. Cell Biol.* **19**, 2846–2852 (1999).
34. Solow, S., Salunek, M., Ryan, R. & Lieberman, P.M. Taf(II) 250 phosphorylates human transcription factor IIA on serine residues important for TBP binding and transcription activity. *J. Biol. Chem.* **276**, 15886–15892 (2001).
35. Bleichenbacher, M., Tan, S. & Richmond, T.J. Novel interactions between the components of human and yeast TFIIA/TBP/DNA complexes. *J. Mol. Biol.* **332**, 783–793 (2003).
36. Woiwode, A. *et al.* PTEN represses RNA polymerase III-dependent transcription by targeting the TFIIIB complex. *Mol. Cell Biol.* **28**, 4204–4214 (2008).
37. Garza, A.M., Khan, S.H. & Kumar, R. Site-specific phosphorylation induces functionally active conformation in the intrinsically disordered N-terminal activation function (AF1) domain of the glucocorticoid receptor. *Mol. Cell Biol.* **30**, 220–230 (2010).
38. Wright, P.E. & Dyson, H.J. Linking folding and binding. *Curr. Opin. Struct. Biol.* **19**, 31–38 (2009).
39. Hoeflich, K.P. & Ikura, M. Calmodulin in action: diversity in target recognition and activation mechanisms. *Cell* **108**, 739–742 (2002).
40. Lee, C.W., Martinez-Yamout, M.A., Dyson, H.J. & Wright, P.E. Structure of the p53 transactivation domain in complex with the nuclear receptor coactivator binding domain of CREB binding protein. *Biochemistry* **49**, 9964–9971 (2010).
41. van Werven, F.J., van Teeffelen, H.A., Holstege, F.C. & Timmers, H.T. Distinct promoter dynamics of the basal transcription factor TBP across the yeast genome. *Nat. Struct. Mol. Biol.* **16**, 1043–1048 (2009).
42. Liu, J. *et al.* Intrinsic disorder in transcription factors. *Biochemistry* **45**, 6873–6888 (2006).
43. Kim, Y., Geiger, J.H., Hahn, S. & Sigler, P.B. Crystal structure of a yeast TBP/TATA-box complex. *Nature* **365**, 512–520 (1993).

ONLINE METHODS

Protein preparation. The fusion protein encoding yTAF1-TAND1-TAND2 (residues 8–71) linked to the core domain of yTBP (residues 61–270) with a $(GGGS)_3$ linker, as well as GST-TAF1-TAND and TBP proteins, were expressed and prepared as previously described[25]. For crystallization, the yeast fusion yTBP-yTAF1 protein was prepared to a final concentration of 1.5 mM in 100 mM NaCl, 0.5 mM TCEP, 10% (v/v) glycerol and 20 mM HEPES, pH 7.5.

Crystallization, data collection and structure determination. Crystals were obtained at 4 °C by sitting-drop vapor diffusion against a well solution containing 0.2 M cesium chloride, 0.1 M MES, pH 6.5, and 26% PEG350MME. A native diffraction data set was collected at the temperature of 100 K from a single crystal diffracting to 1.97 Å at beamline ID14-1 (λ = 0.9334 Å) in ESRF, Grenoble. The initial structure was determined by molecular replacement with Molrep integrated in the CCP4i package[44]. The initial $F_o - F_c$ map revealed the electron density for the yTAND12 domain. No electron density was observed for the $(GGGS)_3$ fusion linker connecting $yTAF1_{71}$ and $yTBP_{61}$ or for residues $yTBP_{61}$, $yTAF1_{67–71}$. The distance between $yTBP_{61}$ and $yTAF_{66}$ in the crystal structure is 38 Å; thus, the disordered fusion linker including flanking disordered residues, which would cover 65 Å in an extended state, comfortably covers this distance. The uncleaved N-terminal hexahistidine tag is also not observed but may have contributed to stabilizing crystallization because no crystals were obtained for the hexahistidine-free fusion-protein construct. The peptide was modeled, and the entire model was manually adjusted with Coot[45]. The models were subjected to several rounds of refinement and validation with autoBUSTER[46] and MolProbity[47], respectively, to obtain the final model. The final model had 98.7% of the residues in the Ramachandran favored region with no Ramachandran outliers. The overall MolProbity score of the final model was of 0.93, and the structure belongs to the best-scoring structures at comparable resolution (100th percentile). Side chain surface accessibility was calculated from the coordinates with VADAR[48]. All protein-structure figures were generated with PyMOL (http://www.pymol.org/).

NMR experiments and data analysis. All NMR experiments were performed with a Varian INOVA spectrometer operating at a proton Larmor frequency of 600 MHz at 25 °C. Data were processed and analyzed as described[49]. Assignments for yTBP-yTAF1 (ref. 50; BMRB 6702) were confirmed and slightly extended by HNCO, HNCA, HN(CO)CA, HN(CA)CB and HN(COCA)CB experiments on a deuterated sample. The ^{15}N R_1 and ^{15}N $R_{1\rho}$ relaxation experiments for yTBP-yTAF1 were recorded with a protein concentration of 320 µM with ^{15}N-^{13}C-^{2}H–labeled protein. For the R_1 relaxation experiments, 18 data points, including four duplicates, were recorded, with relaxation delays between 10 ms and 1,500 ms. The spin-lock field strength used for measurements of $R_{1\rho}$ was 1,730 Hz, and the number of recorded data points was 19 with relaxation delays between 5 ms and 50 ms, including five duplicates. The ^{15}N-^{1}H NOE measurements were performed by recording experiments including or not including a 5-s period of 120° ^{1}H saturation pulses. The total recovery delay was 12 s in both cases. For the evaluation of relaxation data, PINT[51] was used where peaks were integrated by line shape fitting. R_1 and $R_{1\rho}$ rate constants were obtained by fits to exponential functions. The jackknife approach was used for estimation of errors in the decay rates[52]. R_2 was calculated with the following equation: $R_{1\rho} = R_1\cos^2\theta + R_2\sin^2\theta$, where θ is the tilt angle, defined as $\arctan(B_1/\Omega)$. B_1 is the spin-lock field strength, and Ω the resonance offset from the radio frequency carrier[53]. For the calculation of the rotational correlation time (τ_c), Tensor2 was used[54]. The correlation time was calculated from the ratio R_2/R_1 with an axially symmetric rotational diffusion tensor, assuming that the yTBP-yTAF1 protein was arranged as a prolate ellipsoid. Residues with NOE <0.65 were excluded from the analysis.

Yeast strains and plasmid construction. *TAF1* deletion strains, YTK11411 and YTK12029, were described previously[55]. New strains used in this work are summarized in **Supplementary Table 2** and were constructed as follows: YTK12803, YTK13412, YTK13413, YTK13414, YTK13415, YTK13416, YTK13417 and YTK13444 were generated from YTK11411 by replacement of the *URA3*-marked plasmid (pYN1/*TAF1*) with *HIS3*-marked plasmids pM7121/*taf1* ΔTAND, pM7280/*taf1* E60A E62A, pM7281/*taf1* E60A E62A D66A, pM7282/*taf1* E58A D59A, pM7283/*taf1* E58A D59A E60A E62A, pM7284/*taf1* H50A, pM7285/*taf1* H50G and pM7298/*taf1* ΔTAND2, respectively, using a plasmid shuffle technique. Similarly, YTK13428, YTK13429, YTK13430, YTK13431, YTK13432, YTK13433, YTK13434, YTK13435, YTK13436 and YTK13536 were generated from YTK11411 by replacement of pYN1/*TAF1* with *LEU2*-marked plasmids pM7118/*TAF1* (ref. 56), pM7119/*taf1* ΔTAND, pM7286/*taf1* ΔTAND1, pM7287/*taf1* ΔTAND1 E60A E62A, pM7288/*taf1* ΔTAND1 E60A E62A D66A, pM7289/*taf1* ΔTAND1 E58A D59A, pM7290/*taf1* ΔTAND1 E58A D59A E60A E62A, pM7291/*taf1* ΔTAND1 H50A, pM7292/*taf1* ΔTAND1 H50G and pM7320/*taf1* ΔTAND1 F57A, respectively.

pM4770/*TAF1* (ref. 55), which contains the entire *TAF1* sequence including its native promoter and terminator (5.3 kb in total), was subjected to site-specific mutagenesis[57] to create pM7121, pM7279, pM7280, pM7281, pM7282, pM7283, pM7284, pM7285 and pM7319. The oligonucleotides used in this study are listed in **Supplementary Table 3**. The 5.1-kb *Not*I–SalI fragment from pM7121/*taf1* ΔTAND was ligated into the *Not*I/SalI sites of pRS315 (ref. 58) to generate pM7119. pM7286/*taf1* ΔTAND1 was created by replacing the 3.4-kb *Not*I–*Xba*I fragment of pM7118/*TAF1* (ref. 56) with the 3.3-kb *Not*I–*Xba*I fragment of pM7279/*taf1* ΔTAND1. The 2.2-kb *BssH*II–*Xba*I fragments including the mutated TAND2 region were amplified by PCR from pM7280, pM7281, pM7282, pM7283, pM7284, pM7285 and pM7319 with the primer pair TK43-TK125, then ligated into the *BssH*II/*Xba*I sites of pM7286 to generate pM7287, pM7288, pM7289, pM7290, pM7291, pM7292 and pM7320, respectively. The 2.2-kb *BamH*I–*Xba*I fragment of pM977/*taf1* ΔTAND2 (ref. 59) was ligated into the *BamH*I/*Xba*I sites of pRS313 to generate pM7298.

To prepare GST-tagged TAND proteins containing TAND2 mutations, the 198-bp BamHI–EcoRI fragments were amplified from pM7280, pM7281, pM7282, pM7283, pM7284 and pM7285 with the primer pair TK344-T869, then ligated into the BamHI/EcoRI sites of pGEX2T (GE Healthcare), generating pM7305, pM7306, pM7307, pM7308, pM7309 and pM7310, respectively. The plasmids expressing wild-type GST-TAND (pM1431) or wild-type TBP (pM1578) were generated as described previously[59].

GST pulldown assay. Purified TBP (20 pmol) was incubated for 1 h with bacterial lysate expressing GST-TAF1-TAND or GST (20 pmol) in 150 µl of 0.2 M KCl, 20 mM Tris-HCl, pH 7.9, 12.5 mM $MgCl_2$, 0.2 mM EDTA, 10% (v/v) glycerol, 1 mM dithiothreitol and 1 mM phenylmethylsulfonyl fluoride at 4 °C. After incubation with 10 µl of glutathione–Sepharose 4B beads (GE Healthcare) for another 1 h, the beads were washed with 3 × 500 µl buffer as above and boiled in SDS sample buffer, and eluates were separated on SDS-PAGE.

44. Collaborative Computational Project. The CCP4 suite: programs for protein crystallography. *Acta Crystallogr. D Biol. Crystallogr.* **50**, 760–763 (1994).
45. Emsley, P., Lohkamp, B., Scott, W.G. & Cowtan, K. Features and development of Coot. *Acta Crystallogr. D Biol. Crystallogr.* **66**, 486–501 (2010).
46. Blanc, E. *et al.* Refinement of severely incomplete structures with maximum likelihood in BUSTER-TNT. *Acta Crystallogr. D Biol. Crystallogr.* **60**, 2210–2221 (2004).
47. Chen, V.B. *et al.* MolProbity: all-atom structure validation for macromolecular crystallography. *Acta Crystallogr. D Biol. Crystallogr.* **66**, 12–21 (2010).
48. Willard, L. *et al.* VADAR: a web server for quantitative evaluation of protein structure quality. *Nucleic Acids Res.* **31**, 3316–3319 (2003).
49. Andresen, C. *et al.* Transient structure and dynamics in the disordered c-Myc transactivation domain affect Bin1 binding. *Nucleic Acids Res.* **40**, 6353–6366 (2012).
50. Mal, T.K. *et al.* Resonance assignments of 30 kDa complexes of TFIID subunit TAF1 with TATA-binding protein. *J. Biomol. NMR* **33**, 76 (2005).
51. Ahlner, A., Carlsson, M., Jonsson, B.H. & Lundström, P. PINT: a software for integration of peak volumes and extraction of relaxation rates. *J. Biomol. NMR* published online, http://dx.doi.org/10.1007/s10858-013-9737-7 (9 May 2013).
52. Mosteller, F. & Tukey, J.W. *Data Analysis and Regression: A Second Course in Statistics* 133–162 (Addison-Wesley, 1977).
53. Palmer, A.G. III & Massi, F. Characterization of the dynamics of biomacromolecules using rotating-frame spin relaxation NMR spectroscopy. *Chem. Rev.* **106**, 1700–1719 (2006).
54. Dosset, P., Hus, J.C., Blackledge, M. & Marion, D. Efficient analysis of macromolecular rotational diffusion from heteronuclear relaxation data. *J. Biomol. NMR* **16**, 23–28 (2000).
55. Ohyama, Y., Kasahara, K. & Kokubo, T. *Saccharomyces cerevisiae* Ssd1p promotes CLN2 expression by binding to the 5′-untranslated region of CLN2 mRNA. *Genes Cells* **15**, 1169–1188 (2010).
56. Takahashi, H., Kasahara, K. & Kokubo, T. *Saccharomyces cerevisiae* Med9 comprises two functionally distinct domains that play different roles in transcriptional regulation. *Genes Cells* **14**, 53–67 (2009).
57. Kunkel, T.A., Roberts, J.D. & Zakour, R.A. Rapid and efficient site-specific mutagenesis without phenotypic selection. *Methods Enzymol.* **154**, 367–382 (1987).
58. Sikorski, R.S. & Hieter, P. A system of shuttle vectors and yeast host strains designed for efficient manipulation of DNA in *Saccharomyces cerevisiae*. *Genetics* **122**, 19–27 (1989).
59. Takahata, S. *et al.* Identification of a novel TATA element-binding protein binding region at the N terminus of the *Saccharomyces cerevisiae* TAF1 protein. *J. Biol. Chem.* **278**, 45888–45902 (2003).